Published as: *Neuron*. 2009 February 26; 61(4): 527–540.

Dscam Mediates Trans-Synaptic Interactions for Remodeling of Glutamate Receptors in *Aplysia* During *De Novo* and Learning-Related Synapse Formation

Hsiu-Ling Li[1,2], **Ben S. Huang**[2], **Harshad Vishwasrao**[1], **Nadia Sutedja**[2], **Wei Chen**[2], **Iksung Jin**[2], **Robert D. Hawkins**[2,3], **Craig H. Bailey**[2,3,4], and **Eric R. Kandel**[1,2,3,4,*]

[1]Howard Hughes Medical Institute, 1051 Riverside Drive, New York, NY 10032

[2]Department of Neuroscience, College of Physicians and Surgeons of Columbia University, 1051 Riverside Drive, New York, NY 10032

[3]New York State Psychiatric Institute, 1051 Riverside Drive, New York, NY 10032

[4]The Kavli Institute for Brain Sciences, 1051 Riverside Drive, New York, NY 10032

Summary

Trans-synaptic interactions between neurons are essential during both developmental and learning-related synaptic growth. We have used *Aplysia* neuronal cultures to examine the contribution of trans-synaptic signals in both types of synapse formation. We find that during *de novo* synaptogenesis, specific presynaptic innervation is required for the clustering of postsynaptic AMPA-like but not NMDA-like receptors. We further find that the cell adhesion molecule Dscam is involved in these trans-synaptic interactions. Inhibition of Dscam either pre- or postsynaptically abolishes the emergence of synaptic transmission and the clustering of AMPA-like receptors. Remodeling of both AMPA-like and NMDA-like receptors also occurs during learning-related synapse formation and again requires the reactivation of Dscam-mediated trans-synaptic interactions. Taken together, these findings suggest that learning-induced synapse formation recapitulates, at least in part, aspects of the mechanisms that govern *de novo* synaptogenesis.

Introduction

Generation of specific connections between neurons is critical for precise wiring of the central nervous system during both development and learning-induced synapse formation in the mature brain. Several studies have implicated candidate genes in mediating the generation of synapse specificity in the context of development (Hummel et al., 2003; Schmucker et al., 2000; Shen and Bargmann, 2003; Shen et al., 2004; Yamagata et al., 2002). In contrast, little is known about their contribution to activity-dependent synaptic growth and thus, the degree to which these two events may share molecular features in common remains unclear.

To address these questions, we have exploited the elementary monosynaptic sensory neuron (SN) to motor neuron (MN) connections of the gill-withdrawal reflex of *Aplysia*

*Corresponding author: 1051 Riverside Drive, PI annex 651 New York, NY 10032.

reconstituted in culture. This reduced system has several distinct features that are advantageous for these studies. First, SN only make synapses with selective postsynaptic MN (e.g. L7 and LFS MN). SN do not form either inappropriate connections with other cells or with themselves (autapses) (Kleinfeld et al., 1990). Thus, this system is well suited for delineating the molecular mechanisms that underlie the generation of specific neuronal connections. Second, freshly cultured SN and MN normally re-establish their synaptic connections during the first four days in culture (Montarolo et al., 1986). The events that occur during this early period (days 1–4) of the co-culture reflect, at least in part, a developmental program for synaptogenesis. Exposure of the mature 5 day cultures to a single pulse of serotonin (5-HT), a modulatory neurotransmitter that mediates behavioral sensitization *in vivo,* induces short-term facilitation (STF) that lasts minutes to hours. In contrast, five spaced pulses of 5-HT elicit long-term facilitation (LTF) that persists for several days (Montarolo et al., 1986). LTF but not STF is accompanied by growth of new synapses (Bailey et al., 1994; Bailey and Kandel, 1993; Glanzman et al., 1989). Thus, the *Aplysia* SN-MN co-culture allows one to study directly the molecular mechanisms that contribute to both developmental and learning-related synapse formation and to address the question of how each process relates to the other.

We first cloned several glutamate receptors in *Aplysia* and found that specific contact between presynaptic SN and an appropriate postsynaptic MN is required for the clustering of AMPA-like but not NMDA-like receptors during *de novo* synapse formation. The molecular diversity of two sets of molecules, Dscam in *Drosophila* and protocadherins in mammals, makes them attractive candidates for mediating specific recognition during synapse formation (Hummel et al., 2003; Schmucker et al., 2000; Zhan et al., 2004). In *Aplysia*, we found several protocadherin isoforms, but did not detect a vast repertorie of Dscam. Among the neurons we examined, the expression profiles of selective protocadherin isoforms do not display neuronal specificity. However, using selective primers against ApDscam, we detected the Dscam messages in both SN and its cognate L7 postsynaptic MN, but not in mis-matched L11 MN. We further found that postsynaptic Dscam co-localizes with AMPA-like receptors, whereas presynaptic Dscam is localized to stable SN varicosities and to the base of growth cones. During *de novo* synapse formation, both pre- and postsynaptic blockade of Dscam abolishes synaptic transmission and the clustering of AMPA-like receptors, suggesting that Dscam-mediated trans-synaptic interactions are crucial for developmental synapse formation.

In comparison, we found that LTF but not STF is associated with the postsynaptic remodeling of both types of glutamate receptors. However, in contrast to *de novo* synapse formation, this learning-related remodeling of both NMDA-like and AMPA-like receptors requires trans-synaptic interactions between SN and MN. Moreover, at mature synapses, Dscam-mediated trans-synaptic signaling is required for the expression of long-term synaptic plasticity and growth. Blockade of Dscam either pre- or postsynaptically does not interfere with STF or with pre-existing synaptic strength, but does inhibit the induction of LTF and the LTF-associated remodeling of glutamate receptors. Taken together, these data suggest that Dscam-mediated signaling required for remodeling of glutamate receptors is one of the key molecular mechanisms for both developmental and learning-related synaptic growth.

Results

De Novo Synapse Formation

During *de novo* synaptogenesis, clustering of AMPA but not NMDA receptors requires presynaptic input—We first cloned one subunit of NMDA-like receptors and two members of AMPA-like receptors in *Aplysia*. We have classified these glutamate

receptors based on the criteria proposed by Sprengel et al. (2001) and their homology with glutamate receptors from both the pond snail, Lymnaea and vertebrates (details in Supplemental Figure S1). The comparison of our nomenclature and others are listed in Table 3 in the Materials and Methods section. Using single cell RT/PCR and *in situ* hybridization, we found that *Aplysia* sensory neurons, express comparable levels of these glutamate receptors to their target L7 MN as well as to the mismatched L11 MN (Supplemental Figure S1). These data suggest that the failure of SN to make connections with L11 MN must be due to the lack of crucial elements other than glutamate receptors.

To begin to identify the components that mediate the specific trans-synaptic interactions between SN and L7 MN, we next sought to determine how these interactions regulate the distribution of glutamate receptors. We tracked the distribution of NMDA-like receptors fused with EGFP (ApNR1/EFGP). We found that the tagged receptors cluster equally well in the processes of solitary L7 MN or in L7 MN co-cultured with SN (Figure 1A, left and right panels, respectively). These NMDA-like receptors are expressed on the cell surface as demonstrated by immunostaining non-permeabilized cells with anti-GFP antibody (Figure 1B). In contrast, both AMPA-like receptors - ApGluR1/EGFP and ApGluR2/EGFP - displayed a diffuse and gradient distribution along the processes of isolated MN (Figure 1C, top panels). Since the expression of AMPA-like receptors occurred in a gradient along the neurites of solitary MN, we acquired images under conditions of higher laser power in order to clearly display the overall distribution of AMPA-like receptors. We observed the same diffuse distribution of AMPA-like receptors in isolated MN using different laser intensities, suggesting that this diffuse distribution is not an artifact of signal saturation (Figure 1C, middle panels). This diffuse distribution was converted to a distinct punctate array when the SN innervate the MN in co-culture (Figure 1C, bottom panels). Moreover, these AMPA-like receptors are targeted to the cell surface as demonstrated by immunostaining non-permeabilized cells with anti-GFP antibody (Figure 1C, right panels). Together, these data suggest that during *de novo* synapse formation, the clustering of AMPA-like, but not NMDA-like receptors requires presynaptic innervation.

To verify this observation, we performed two additional experiments. First, we determined whether elimination of the presynaptic inputs at an established SN to MN synapse would trigger dispersion of the AMPA-like receptor clusters in L7 MN. We found that both subunits of AMPA-like receptors cluster throughout the neurites (Figure 1D, left panels). To eliminate the presynaptic neuron, we injected media into the cell body of SN and followed over time the changes in the distribution of AMPA-like receptors. Concomitant with the death of the presynaptic cell, the AMPA-like receptor puncta gradually dispersed, resulting in a more diffuse receptor distribution similar to the pattern observed on isolated MN (Figure 1D, right middle and bottom panels). This dispersion became prominent at 4 days after denervation and lasted the duration of the experiment (6 days after denervation). By contrast, the distribution of AMPA-like receptors remained punctate over the same time period in MN co-cultured with intact SN (Figure 1D, top right panels).

Second, we co-expressed NMDA-like receptors tagged with the red fluorescent protein (RFP) and AMPA-like receptors/GFP in the L7 MN cultured alone. The AMPA-like receptors distributed homogeneously, whereas NMDA-like receptors formed discrete clusters (Figure 1E, left column and for full size images, see Supplemental Images). We next asked: Do postsynaptic glutamate receptors cluster in a target neuron-specific manner? We found that in response to SN innervation, both AMPA-like and NMDA-like receptors cluster along the neurites of L7 MN, and that most of the AMPA-like punctate structures co-localize with NMDA-like clusters (Figure 1E, middle column and for full size images, see Supplemental Images). In contrast, the AMPA-like, but not NMDA-like receptors failed to form discrete puncta in the mismatched L11 MN innervated by SN (Figure 1E, right column

and for full size images, see Supplemental Images). Together, these findings suggest that during *de novo* synapse formation, specific recognition between synaptically-related pre- and postsynaptic cells is required for the clustering of two AMPA-like receptor subunits but not for the clustering of NMDA-like receptors.

Dscam is commonly expressed in synaptically-related neurons—Precise alignment of the pre- and postsynaptic compartment is thought to rely on the binding specificities of cell adhesion molecules. The complex genomic organization of the protocadherin family in mammals and the extensive alternative splicing of Dscam in *Drosophila* have made them attractive candidates for synaptic recognition because each of these families is capable of generating a large number of isoforms and each of these isoforms might, in turn, contribute to the specificity of neuronal recognition via its specific binding activity (Schmucker et al., 2000; Wu and Maniatis, 1999). We therefore asked: Do protocadherins and Dscam have a role in the clustering of glutamate receptors at *Aplysia* SN-MN synapses? To address this question, we have identified several isoforms of *Aplysia* homologues of protocadherins and Dscam that display a domain organization similar to their mammalian and *Drosophila* homologues, respectively (Figure 2A). The *Aplysia* protocadherins contain 6 or 7 cadherin domains followed by a transmembrane domain, whereas the *Aplysia* Dscam (ApDscam) consists of 10 Immunoglobulin (Ig) domains, 6 fibronectin type III (FN III) domains, and a transmembrane domain (TM) followed by an intracellular domain. We next characterized the expression patterns of these Dscam and protocadherin isoforms in a variety of *Aplysia* neurons by single cell RT/PCR. We did not observe any difference in the expression of five different isoforms of protocadherins in SN or the MN L7 and L11, suggesting that these isoforms might have a role in cell adhesion rather than in neuronal selection at *Aplysia* SN-MN synapses (Figure 2A). This observation does not exclude the possibility that other protocadherins that we have not yet identified might be involved in target selection.

In *Drosophila*, a vast repertoire of Dscam isoforms can be generated by alternative splicing. We next sought to determine whether *Aplysia* neurons also express a large number of Dscam isoforms by performing RT/PCR using the total ganglia RNA as templates. In contrast to the fly Dscam, we did not detect a large collection of *Aplysia* Dscam isoforms. Thus, the proliferation of splice isoforms of Dscam appears to be specific to the insect lineage, as neither vertebrates nor mollusks show evidence for this event. (Agarwala et al., 2001; Barlow et al., 2001).

Although the vertebrate Dscam lacks the molecular diversity, Dscam and its paralogue, Dscam L1 are differentially expressed in various regions of the mouse CNS (Barlow et al., 2002). For instance, Dscam and Dscam L1 are inversely expressed in the ventral and dorsal spinal cord. In the adult cortex, Dscam is predominantly expressed in layer 3/5 pyramidal neurons, whereas Dscam L1 is expressed in layer 2 granule cells. This suggests that mammalian Dscam, even in the absence of a repertoire of isoforms, might have the same but perhaps more restricted role in neuronal specification or recognition. We therefore sought to determine whether there is any correlation in the expression of ApDscam in synaptically-related neurons. Using a panel of primers against various regions of ApDscam, we performed single cell RT/PCR to determine the expression of Dscam in SN, L7 and L11 MN (Figure 2A). When one set of primers flanking the Ig7 domain of ApDscam was used for single cell RT/PCR, we detected comparable signals in *Aplysia* SN and L7 but not in mismatched L11 MN (Figure 2A, primer set 1). By contrast, we detected comparable signals in SN, L7 and L11 MN using the primer sets covering the Ig6 and N-terminal half of Ig7 domains of ApDscam (Figure 2A, primer set 2). These data suggest that the ApDscam on L11 might be different from that on L7 in the Ig7 domain of ApDscam. To test this possibility, we directly amplified the Ig7 domain from SN, L7 and L11 MN (Figure 2A,

primer set 3). We found that SN, L7 and L11 MN express comparable amounts of the Ig7 domain by single cell RT/PCR. In this experiment, the primer set 4 covering the Ig9 and FNIII domain was used for internal control (Figure 2A). Based on the sequencing results, we did not observe any diversity in the Ig7 domain of *Ap*Dscam. Together, primer set 1 failed to amplify the ApDscam (encoding a.a. 536-717) from L11 MN, but not from SN or L7 MN, whereas primer set 2 and 3 could amplify the segment encoding a.a 560-686 and a.a. 634-722 from these three types of neurons. These data suggest that unlike *Drosophila* Dscam 2, the difference in ApDscam on L7 and L11 most likely is not due to diversity of the Ig7 domain. The difference resides in a region before the Ig7 domain (between a.a. 536 and 560 or between nt 1608 and 1680) (Figure 2A).

We next asked: Does this ApDscam only participate in the formation of glutamatergic excitatory connections, such as the synapses between SN and L7 MN or does it also participate in the formation of connections mediated by other transmitters, such as the dual excitatory and inhibitory synaptic connections between the cholinergic interneuron L10 and L7 MN? We therefore examined the expression of ApDscam in interneuron L10. We found that the expression level of ApDscam in interneuron L10 is comparable to that in both SN and L7 MN (Figure 2A), suggesting that matched expression of Dscam in synaptically-related neurons is not restricted to the chemical nature of synaptic transmission.

Postsynaptic Dscam is required during *de novo* synaptogenesis for the remodeling of AMPA receptors—We next sought to test the role of Dscam in *de novo* synapse formation. We reasonsed that it might be difficult to block the extracellular binding activity of Dscam since there might be as-yet identified Dscam isoforms or paralogues on SN and L7 MN, even though we did not detect a molecular diversity of Dscam so far. Thus, we first knocked down the signaling cascade downstream of Dscam by over-expressing the intracellular domain of Dscam (INDscam) in L7 MN. INDscam contains several putative binding sites for SH2 and SH3 domains such as YDXX and PXXP motifs as well as PKC binding sites, even though this region of Dscam is not highly homologous between species. We found that postsynaptic over-expression of INDscam in immature SN-MN co-cultures blocked both the clustering of AMPA-like receptors and synaptic transmission (panel (II) in Figure 2B, see Supplemental Images for full size images. Both quantification of receptor clustering and electrophysiological results are at the bottom of the charts). However, over-expression of this truncated mutant had no effect on the clustering of NMDA-like receptors (panel (III) in Figure 2B and Supplemental Images), even when the expression level of INDscam was higher than that required to abolish the clustering of AMPAR (panel II). This demonstrates that the blockade is receptor specific. In addition, we showed that AMPA-like receptors co-localize with wild type Dscam (WTDscam), further suggesting that Dscam is required for the clustering of AMPA-like receptors (Figure 2C).

Since it is possible that INDscam might interfere with signaling pathways other than those downstream of Dscam, we next determined: 1) whether co-expression of WTDscam/RFP with INDscam/EGFP could rescue the competence for synapse formation and 2) whether knocking down the expression of Dscam by RNAi could affect synapse formation as measured physiologically. We found that over-expression of WTDscam/RFP indeed rescued the effects of INDscam/EGFP on synapse formation (Figure 2B, bottom chart). This rescue is specific since over-expression of WTDscam/RFP alone did not alter synaptic transmission (Figure 2B, bottom chart). We further used RNAi to determine the effects of knocking down the expression of Dscam on synapse formation. We first performed single cell RT-PCR to determine the specificity and kinetics of these RNAi on the expression of Dscam. We found that the RNA levels of Dscam were selectively decreased at 12h, 24h, and 48h after injecting a mixture of 3 different Dscam-targeted RNAi into SN or MN, but these RNAi had no effect on the expression of two synaptic markers, AMPA receptors and synapsin (Supplemental

Figure S4). Moreover, injection of a mixture of 3 control RNAi had no effect on the RNA levels of Dscam. We then injected a mixture of these ApDscam-targeted RNAi into either presynaptic SN or postsynaptic MN every 48 h and measured the strength of synaptic transmission between SN and MN synapses after 5 days in culture. Knocking down the expression of both pre- and postsynaptic Dscam abolished the evoked synaptic transmission (bottom right panel, Figure 2B), suggesting that Dscam is essential for the formation of SN and MN synapses.

During *de novo* synapse formation, Dscam is associated with the anchorage of growth cones and the stabilization of presynaptic varicosities—We next sought to determine the role of presynaptic Dscam in *de novo* synapse formation. Consistent with previous results, SN only form synaptic connections with L7 but not L11 MN (Figure 3A). However, over-expression of INDscam in SN co-cultured with L7 MN abolishes the emergence of synaptic transmission in the SN-L7 MN synapses (Figure 3A).

We next monitored changes in the distribution of a fusion construct WTDscam/EGFP in SN innervating L7 or L11 MN (Wang et al., 2004). SN and MN were also filled with the whole cell markers, dextran Alexa 555 and 680, respectively to label the full morphology of both pre- and postsynaptic cells. We imaged the distribution of WTDscam/EGFP in relation to the structural changes and these data are presented in Supplemental Videos 1–4. We found that during *de novo* synapse formation, SN neurites were either immobile or displayed rapid extension or retraction (Supplemental Video 1). In the actively growing neurites, WTDscam/EGFP was highly enriched at the base of growth cones and appeared to serve as an anchor for filopodia at the leading edge that sprout new neuritic growth (Figure 3B and Supplemental Video 1 and Sub-video 1.2). When neurites stop growing and become stationary, a high concentration of WTDscam/EGFP accumulated at their tips (Supplemental Sub-video 1.1). The rapidly growing axons of SN appear to use the same strategy for navigation whether co-cultured with L7 or L11 MN, even though SN lose their directionality when paired with L11 MN (Supplemental Videos 1–4 and Figure 3C).

Although most of the WTDscam/EGFP followed growth cones traveling down the postsynaptic processes, some of the presynaptic varicosities retained high levels of WTDscam/EGFP locally but only when SN were co-cultured with L7 and not with L11 MN (Figure 3C and Supplemental Videos 1–4). Interestingly, these WTDscam/EGFP-enriched presynaptic varicosities were stable morphologically (in SN-L7 MN co-cultures), whereas presynaptic varicosities with no detectable WTDscam/EGFP signals were more labile over the course of our time-lapse recordings (most varicosities in SN-L11MN co-cultures in Figure 3C and Supplemental Videos 1–4 and two neighboring varicosities in SN-L7 MN co-culture Sub-video 1.3).

We also tracked the distribution of Protocadherin 1 which, in contrast to Dscam, is expressed on SN, L7 and L11 MN. We found that Protocadherin/EGFP (Pcdh/EGFP) was most often targeted to the tips rather than the base of growth cones in actively extending SN neurites which innervated either L7 or L11 MN (Figure 3D, Supplemental Videos 5–8). Moreover, the presence or absence of Pcdh/EGFP was not directly associated with the stability of presynaptic varicosities (Figure 3E and Supplemental Videos 5–8). Together, these data suggest that the differential distribution of Dscam and protocadherin during the extension of SN neurites (summarized in Table 1) might reflect a difference in their functional contribution to *de novo* synapse formation in *Aplysia* neuronal culture.

Learning-Related Synapse Formation

Dscam is highly expressed in regions of the adult mammalian brain that are involved in learning and memory such as cortex and hippocampus (Agarwala et al., 2001; Barlow et al.,

2001). However, the contribution of Dscam to the expression of long-term plasticity and learning-related synapse formation has not been explored. We therefore repeated the experiments described above but now in mature *Aplysia* SN-MN synapses following the induction of short-term or long-term plasticity.

Long-term but not short-term facilitation is accompanied by the remodeling of glutamate receptors—We first determined whether treatment with 5-HT could induce the remodeling of glutamate receptors at the *Aplysia* SN-MN synapse. As we demonstrated above (Figure 1A), NMDA-like but not AMPA-like receptors formed clusters even in the absence of presynaptic SN (Figure 4A and 4B, top panels). Induction of LTF (by five 5-min pulses of 5-HT with 15-min intervals) but not STF (10 min after treatment with one single pulse of 5-HT) led to a 2-fold increase in the number of both NMDA and AMPA receptor clusters at 12 h after stimulation (Figure 4A and 4B, middle and bottom panels). However, this remodeling required information from presynaptic cells since it occured only when MN were innervated by SN (Figure 4A and 4B, bottom panels),

The 5-HT induced changes in glutamate receptors co-localize with presynaptic markers—We next sought to determine whether the LTF-induced modulation of glutamate receptors co-localizes with presynaptic markers at the SN-MN synapses. We examined this in two ways: 1) we expressed simultaneously both Apsynapsin/RFP in SN and ApGluR1/EGFP in L7 MN (Figure 5A) and 2) we expressed Apsynapsin/EGFP in SN only and cells were immunostained with antibodies against *Aplysia* glutamate receptors after treatment with 5-HT. We found AMPA-like receptors clustered along the processes of L7 MN and approximately 30% of these postsynaptic receptor clusters were co-localized with synapsin prior to stimulation (left panels in Figure 5B and 5C and see Supplemental Images for full size results). The cell bodies, but not the processes of *Aplysia* neurons are prone to emit autofluorescence (Figure 5B). In Figure 5, this autofluorescence is detectable with EGFP but not RFP signals. In response to five repeated pulses of 5-HT, we observed a pronounced and perhaps coordinated redistribution of both presynaptic synapsin and postsynaptic AMPA-like receptors 24 hr after training (right panels in Figure 5B and 5C and see Supplemental Images for full size images). Consistent with our previous results, there is a high percentage of non-colocalized signals outside of the major processes of L7 MN (pink arrowheads, Figure 5), whereas the signals along the initial segment of L7 MN (insets) have a higher percentage of co-localization (blue arrowheads, Figure 5).

Immunostaining also allowed us to monitor the LTF-induced remodeling of endogenous glutamate receptors. Since *Aplysia* neurons are not highly polarized (receptive and transmissive surfaces are often closely juxtaposed), the interpretation of double staining with both pre- and postsynaptic markers can be difficult. Thus, we expressed ApSynapsin/EGFP in SN that were co-cultured with L7 MN. We found that induction of LTF was associated with the formation of new SN varicosities at 24 h after 5 pulses of 5-HT (Supplemental Figure S3A and S3B). These new 5-HT-induced varicosities co-localized with discrete puncta of immunoreactivity detected by anti-NMDA and anti-AMPA receptor antibodies (Supplemental Figure S3A and S3B; see Figure S2 for antibody specificity).

Postsynaptic Dscam is required for the remodeling of AMPA receptors during learning-related synapse formation—Does Dscam-mediated trans-synaptic recognition also have a role in the glutamate receptor re-organization that occurs with the induction of LTF? To address this question, we expressed ApGluR2/RFP postsynaptically in 1-day old co-cultures to allow the clustering of AMPA-like receptors and the establishment of synapses. When the culture had grown for 4 days, we expressed in the same L7 MN, either EGFP or INDscam/EGFP. We then treated the cells with either 1 pulse or 5 pulses of 5-HT to induce STF or LTF, respectively. Consistent with previous results, induction of STF

did not trigger any discernible remodeling of ApGluR2/RFP in cultures that expressed either EGFP or INDscam/EGFP (Figure 6A, third panels). In contrast, the expression of INDscam/EGFP but not EGFP prevented the remodeling of ApGluR2/RFP and the expression of LTF induced by treatment with 5 pulses of 5-HT (Figure 6A, bottom panels and Table 2, LTF(II)(1,3)). The effects of INDscam/EGFP on the induction of LTF was rescued by co-expression with WTDscam/RFP postsynaptically, whereas over-expression of WTDscam/RFP alone had no effects on the expression of LTF (Table 2, LTF(II)(4) and (II)(2)). Moreover, knocking down the expression of Dscam by Dscam-targeted RNAi abolished 5-HT induced LTF, but not STF (Table 2, LTF(II)(8)(10) and STF(II)(5)(6)), whereas the control RNAi had no effect on the expression of LTF (Table 2, LTF(II)(7)(9)). In the absence of 5-HT, both Dscam-targeted RNAi and INDscam did not alter the basal EPSP during the same time period (Table 2, LTF(I)(3,5)), suggesting Dscam-targeted RNAi blocked selectively 5-HT-induced LTF. Together, these data suggest that the induction of LTF recapitulates, at least in part, aspects of the developmental program and that Dscam-mediated trans-synaptic signaling is a common molecular mechanism shared by both *de novo* and learning-related synapse formation.

LTF but not STF is associated with presynaptic remodeling of Dscam and Protocadherin—Does presynaptic Dscam also contribute to the expression of LTF and learning-related synaptic growth? We found that presynaptic over-expression of INDscam in mature SN-MN synapses selectively inhibited LTF but not STF (Table 2, LTF(II)(5) and STF(II)(3)). This effect can be rescued by co-expression with WTDscam in the presynaptic SN (Table 2, LTF(II)(6)). Similarly, knocking down the expression of presynaptic Dscam by Dscam-targeted RNAi blocked 5-HT-induced LTF, but not STF (Table 2, LTF(II)(9,10) and STF(II)(6)). We further found that in response to the induction of LTF, the WTDscam/EGFP aggregates at the axonal terminals of stationary neurites dissolved over time into finer puncta. The dissolution of the WTDscam/EGFP at the terminal SN varicosities converted the stationary neurites into mobile ones and, in many instances, allowed the sprouting of axonal filopodia (Figure 6B, right panels and Supplemental Video 9 and Sub-video 9.1). This phenomenon was detectable as early as 3 hr after treatment with five repeated pulses of 5-HT. We also observed the formation of new varicosities that over time became enriched in WTDscam/EGFP (Figure 6B, left panels and Supplemental Video 9 and Sub-video 9.2). Consistent with our previous results (Figure 3D and Supplemental Video 2), these varicosities were morphologically stable. In comparison, induction of LTF triggered targeting of protocadherin to the tips of SN neurites prior to sprouting of new filopodia (Figure 6D, left panels and Supplemental Video 11). By contrast, exposure to 1 pulse of 5-HT did not induce any detectable synaptic remodeling of either WTDscam/EGFP or protocadherin/EGFP (Figure 6C and D, right panels and Supplemental Videos 10 and 12).

Discussion

AMPA but not NMDA receptors cluster in response to innervation

We have found that clustering of NMDA receptors occurs even in the absence of presynaptic inputs. By contrast, both the initiation and the maintenance of AMPA receptor clusters require a specific interaction between the presynaptic SN and the postsynaptic MN. These results are consistent with previous reports in solitary hippocampal GABAergic neurons that have shown that glutamate inputs are required for the clustering of endogenous AMPA receptors but not NMDA receptors (Rao et al., 2000). Our data are also in agreement with the findings that NMDA clusters are present on the surface of cortical neurons prior to synapse formation. Furthermore, the recruitment of NMDA receptors to the synaptic sites occurs with faster kinetics than that of AMPA receptors (Washbourne et al., 2002; Washbourne et al., 2004).. Finally, our results suggest the possibility of postsynaptic silent

synapses in *Aplysia* that express abundant NMDA receptors but few AMPA receptors, much as is the case in the mammalian brain

A possible role of Dscam in neuronal recognition and the generation of synapse specificity

Dscam has been found to be critical for the repulsion of sister branches during axonal segregation in the fly and vertebrate retina (Fuerst et al., 2008; Hattori et al., 2007; Hughes et al., 2007; Matthews et al., 2007; Millard et al., 2007; Soba et al., 2007; Wojtowicz et al., 2007). However, Dscam also seems to act as an attractive cue in axonal guidance and in the formation of lamina-specific connections in vertebrates (Hummel et al., 2003; Sanes et al., 2008; Stein., 2008). We have tested both possibilities. We did not observe any defects in neuritic branching in *Aplysia* neurons overexpressing INDscam or RNAi (data not shown). However, we found that Dscam often accumulated in SN varicosities contacting L7 MN, but not L11 MN and that this retention correlated with the stability of the varicosities, suggesting ApDscam might function as an attractive cue in the Aplysia SN-MN synapses. Using selective primers covering the Ig 6 domain of ApDscam, we were able to amplify ApDscam signals on SN and L7 MN, but not on L11 MN (Figure 2A). It is possible that the Dscam mRNA in L11 MN might lack part of Ig 6 domain, all of Ig 6 domain, or the entire sequences above Ig 7 domain. Thus, whether L11 MN express fully functional Dscam and the nature of the L11-specific Dscam protein await further analysis. Answers to these questions would help us to better understand whether Dscam is causally involved in the generation of synapse specificity. Nonetheless, Dscam could perform either attractive or repulsive functions in a context-dependent fashion.

LTF but not STF is associated with the remodeling of postsynaptic glutamate receptors

We found that induction of LTF but not STF is associated with postsynaptic redistribution of NMDA-like and AMPA-like receptors. We further found that the 5-HT-induced remodeling of glutamate receptors requires presynaptic innervation. This is consistent with previous findings that treatment with repeated pulses of 5-HT only enhances glutamate sensitivity on those regions of the postsynaptic target directly opposed to presynaptic SN varicosities, but has no effect on isolated MN (Zhu et al., 1997). By contrast, Chitwood et al. (2001) found that the application of brief pulses of glutamate combined with a 10 min exposure to 5-HT was sufficient to induce an increase in the postsynaptic glutamate sensitivity of solitary MN *in vitro.* This facilitatory effect occured within minutes. Methodological differences between our experiments and those of Chitwood et al. might explain in part the apparent discrepancy in the kinetics of the remodeling of postsynaptic glutamate receptors and in the requirement of presynaptic neurons for this event.

Learning-related synapse formation recapitulates the developmental program for re-establishment and maintenance of neuronal connectivity

Our data suggests that Dscam-mediated trans-synaptic interactions might contribute to *de novo* and learning-related synapse formation via at least two different but coordinated mechanisms (Figure 7). First, prior to innervation, NMDA receptors cluster randomly along the postsynaptic surface. In response to specific and appropriate innervation, postsynaptic Dscam promotes the recruitment of glutamate receptors, especially AMPA receptors. In contrast to postsynaptic Dscam, the majority of presynaptic Dscam is found in axonal growth cones traveling along their postsynaptic target cells but some Dscam signal is retained in a subset of stable varicosities. During *de novo* synapse formation, this transient accumulation of Dscam, and potentially other cell adhesion molecules, might confer neuronal specificity at selected presynaptic varicosities that are stabilized at specific postsynaptic sites where both Dscam and glutamate receptors are enriched (Figure 7).

Interestingly, induction of LTF re-utilizes the Dscam-mediated trans-synaptic interactions to regulate the remodeling of postsynaptic glutamate receptors. LTF triggers the dissolution of presynaptic Dscam at terminal varicosities on the one hand, and the accumulation of Dscam in 5-HT-induced newly formed presynaptic varicosities on the other. The redistribution of Dscam at terminal varicosities permits the outgrowth of new filopodia and may provide additional guidance cues required for the local pathfinding of these filopodia. The enrichment of Dscam in the 5-HT-induced newly formed varicosities appears to stabilize these presynaptic structures at defined postsynaptic sites and may promote the subsequent assembly and maturation of new synaptic connections. Thus, the reactivation of Dscam-mediated trans-synaptic signaling during learning-related synapse formation could reflect an important molecular mechanism by which the precise wiring of neuronal networks is preserved in the adult brain.

Materials and Methods

Electrophysiology

The EPSPs were measured by intracellular recordings as previously described (Udo et al., 2005). Briefly, both SN and MN were impaled with sharp microelectrodes (8–10mΩ) containing 2.5 M KCl. The MN was held at a potential of −30mV below its resting potential. The SN was then stimulated with depolarizing pulses to fire an action potential and the evoked EPSP in the MN was recorded.

Single Cell PCR

SN and MN were isolated and placed onto poly-L-lysine coated cover glasses with dimensions of about 2×2 mm for 5 days prior to experiments. Single cell PCR was performed based on the protocols described before (Dulac and Axel, 1995). All PCR products were subject to sequencing analysis. The primers used to amplify the corresponding fragment of the genes were listed in Table 5.

Quantitative analysis of fluorescently-labeled glutamate receptors

An algorithm was designed for the quantitative study of the clusters of glutamate receptors and Dscam. Using this program, the threshold intensity for each image was estimated based on the histograms and statistics of individual pixels in user selected polygonal regions. Different polygonal regions on each image were chosen and quantified to ensure an unbiased quantification of the clusters of glutamate receptors along the neurites. This quantitative procedure was performed repeatedly and different polygonal regions were chosen each time until the analysis covered most of the neurites in each image. The number of the punctate structures in each culture condition was then generated automatically after analysis.

Another customized algorithm was programmed for the analysis of co-localization. Based on the scale of the images, the user defined the diameter (μm) of the smallest and largest bounding circle for accepted puncta (e.g. 1 pixel=0.3 μm for the images in Figure 1F). The user then set the threshold intensity above which possible puncta were defined (e.g. 100 pixel for the images in Figure 1F). This program then generated a list of good puncta automatically. In any given experiments, the same parameters were applied for the analysis of both green and red signals. The lists of good puncta were saved in separate files. We then commanded the program to co-localize these files and the number of overlapping puncta of green and red signlas was counted.

Supplementary Material

Refer to Web version on PubMed Central for supplementary material.

Acknowledgments

We thank Drs. Larry Zipursky, Kelsey Martin and members of the Kandel lab for critical reading of the manuscript and helpful discussion. Mr. Leonard Zablow for assistance with the imaging analysis;. This work was supported by grants from HHMI to E.R.K. and the Kavli Institute for Brain Sciences.

References

Agarwala KL, Ganesh S, Amano K, Suzuki T, Yamakawa K. DSCAM, a highly conserved gene in mammals, expressed in differentiating mouse brain. Biochem Biophys Res Commun. 2001; 281:697–705. [PubMed: 11237714]

Bailey CH, Alberini C, Ghirardi M, Kandel ER. Molecular and structural changes underlying long-term memory storage in Aplysia. Adv Second Messenger Phosphoprotein Res. 1994; 29:529–544. [PubMed: 7848731]

Bailey CH, Kandel ER. Structural changes accompanying memory storage. Annu Rev Physiol. 1993; 55:397–426. [PubMed: 8466181]

Barlow GM, Micales B, Chen XN, Lyons GE, Korenberg JR. Mammalian DSCAMs: roles in the development of the spinal cord, cortex, and cerebellum? Biochem Biophys Res Commun. 2002; 293:881–891. [PubMed: 12051741]

Barlow GM, Micales B, Lyons GE, Korenberg JR. Down syndrome cell adhesion molecule is conserved in mouse and highly expressed in the adult mouse brain. Cytogenet Cell Genet. 2001; 94:155–162. [PubMed: 11856873]

Dulac C, Axel R. A novel family of genes encoding putative pheromone receptors in mammals. Cell. 1995; 83:195–206. [PubMed: 7585937]

Fuerst PG, Koizumi A, Masland RH, Burgess RW. Neurite arborization and mosaic spacing in the mouse retina require DSCAM. Nature. 2008; 451:470–474. [PubMed: 18216855]

Glanzman DL, Kandel ER, Schacher S. Identified target motor neuron regulates neurite outgrowth and synapse formation of aplysia sensory neurons in vitro. Neuron. 1989; 3:441–450. [PubMed: 2642005]

Hattori D, Demir E, Kim HW, Viragh E, Zipursky SL, Dickson BJ. Dscam diversity is essential for neuronal wiring and self-recognition. Nature. 2007; 449:223–227. [PubMed: 17851526]

Hughes ME, Bortnick R, Tsubouchi A, Baumer P, Kondo M, Uemura T, Schmucker D. Homophilic Dscam interactions control complex dendrite morphogenesis. Neuron. 2007; 54:417–427. [PubMed: 17481395]

Hummel T, Vasconcelos ML, Clemens JC, Fishilevich Y, Vosshall LB, Zipursky SL. Axonal targeting of olfactory receptor neurons in Drosophila is controlled by Dscam. Neuron. 2003; 37:221–231. [PubMed: 12546818]

Kleinfeld D, Parsons TD, Raccuia-Behling F, Salzberg BM, Obaid AL. Foreign connections are formed in vitro by Aplysia californica interneuron L10 and its in vivo followers and non-followers. J Exp Biol. 1990; 154:237–255. [PubMed: 2277259]

Matthews BJ, Kim ME, Flanagan JJ, Hattori D, Clemens JC, Zipursky SL, Grueber WB. Dendrite self-avoidance is controlled by Dscam. Cell. 2007; 129:593–604. [PubMed: 17482551]

Millard SS, Flanagan JJ, Pappu KS, Wu W, Zipursky SL. Dscam2 mediates axonal tiling in the Drosophila visual system. Nature. 2007; 447:720–724. [PubMed: 17554308]

Montarolo PG, Goelet P, Castellucci VF, Morgan J, Kandel ER, Schacher S. A critical period for macromolecular synthesis in long-term heterosynaptic facilitation in Aplysia. Science. 1986; 234:1249–1254. [PubMed: 3775383]

Rao A, Cha EM, Craig AM. Mismatched appositions of presynaptic and postsynaptic components in isolated hippocampal neurons. J Neurosci. 2000; 20:8344–8353. [PubMed: 11069941]

Schmucker D, Clemens JC, Shu H, Worby CA, Xiao J, Muda M, Dixon JE, Zipursky SL. Drosophila Dscam is an axon guidance receptor exhibiting extraordinary molecular diversity. Cell. 2000; 101:671–684. [PubMed: 10892653]

Shen K, Bargmann CI. The immunoglobulin superfamily protein SYG-1 determines the location of specific synapses in C. elegans. Cell. 2003; 112:619–630. [PubMed: 12628183]

Shen K, Fetter RD, Bargmann CI. Synaptic specificity is generated by the synaptic guidepost protein SYG-2 and its receptor, SYG-1. Cell. 2004; 116:869–881. [PubMed: 15035988]

Soba P, Zhu S, Emoto K, Younger S, Yang SJ, Yu HH, Lee T, Jan LY, Jan YN. Drosophila sensory neurons require Dscam for dendritic self-avoidance and proper dendritic field organization. Neuron. 2007; 54:403–416. [PubMed: 17481394]

Udo H, Jin I, Kim JH, Li HL, Youn T, Hawkins RD, Kandel ER, Bailey CH. Serotonin-induced regulation of the actin network for learning-related synaptic growth requires Cdc42, N-WASP, and PAK in Aplysia sensory neurons. Neuron. 2005; 45:887–901. [PubMed: 15797550]

Washbourne P, Bennett JE, McAllister AK. Rapid recruitment of NMDA receptor transport packets to nascent synapses. Nat Neurosci. 2002; 5:751–759. [PubMed: 12089529]

Washbourne P, Liu XB, Jones EG, McAllister AK. Cycling of NMDA receptors during trafficking in neurons before synapse formation. J Neurosci. 2004; 24:8253–8264. [PubMed: 15385609]

Wojtowicz WM, Wu W, Andre I, Qian B, Baker D, Zipursky SL. A vast repertoire of Dscam binding specificities arises from modular interactions of variable Ig domains. Cell. 2007; 130:1134–1145. [PubMed: 17889655]

Wu Q, Maniatis T. A striking organization of a large family of human neural cadherin-like cell adhesion genes. Cell. 1999; 97:779–790. [PubMed: 10380929]

Yamagata M, Weiner JA, Sanes JR. Sidekicks: synaptic adhesion molecules that promote lamina-specific connectivity in the retina. Cell. 2002; 110:649–660. [PubMed: 12230981]

Zhan XL, Clemens JC, Neves G, Hattori D, Flanagan JJ, Hummel T, Vasconcelos ML, Chess A, Zipursky SL. Analysis of Dscam diversity in regulating axon guidance in Drosophila mushroom bodies. Neuron. 2004; 43:673–686. [PubMed: 15339649]

Zhu H, Wu F, Schacher S. Site-specific and sensory neuron-dependent increases in postsynaptic glutamate sensitivity accompany serotonin-induced long-term facilitation at Aplysia sensorimotor synapses. J Neurosci. 1997; 17:4976–4986. [PubMed: 9185535]

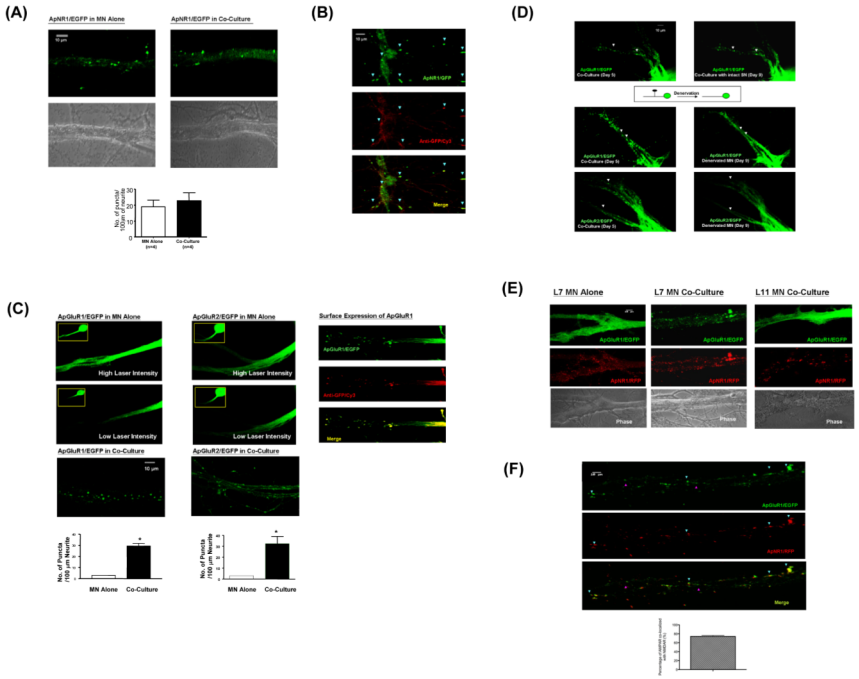

Figure 1.

Clustering of AMPA-like but not NMDA-like receptor requires presynaptic inputs during *de novo* synapse formation. (A) ApNR1/EGFP clusters distribute along the entire neuritic arbors of postsynaptic L7 MN alone and co-cultured with SN (left and right panels, respectively). Unless otherwise specified, the quantification of the numbers of glutamate receptor clusters in this study was performed using an algorithm described in *Materials and Methods*. The results are expressed as the mean numbers of puncta per 100 μm of neurite ± standard error (19±4.203 and 22.75±4.958 puncta in L7 MN alone and co-cultured with SN, respectively. There is no statistical difference between these two groups by a two-sample t test, $p>0.05$, n=4). (B) NMDA-like receptors are targeted to the membrane even in the absence of presynaptic neurons. Isolated L7 MN that express ApNR1/EGFP were fixed under non-permeabilized condition. Surface expression of ApNR1/EGFP was detected using anti-GFP antibody followed by Cy3-conjugated secondary antibody (arrowheads). (C) ApGluR1/EGFP or ApGluR2/EGFP was expressed into L7 MN in the absence or presence of SN (left and right columns, respectively). Both ApGluR1 and ApGluR2 show diffuse and gradient distribution along the processes of solitary MN using both high and low laser intensity (5 mW and 1.5 mW respectively) at the same sample (top and middle panels). The images acquired under lower magnification are shown in insets. By contrast, both subunits of AMPA-like receptors form distinctive puntate structures along the neurites of L7 MN when innervated by SN (bottom panels). Surface expression of ApGluR1 was detected using anti-GFP antibody followed by Cy3-conjugated secondary antibody (right panels). In L7 MN alone, the number of puncta per 100 μm of neurites is 3±0.2 for both ApGluR1, n=6 and ApGluR2, n=7, whereas they are 29.41±2.324, n=10, for ApGluR1 and 32.38±6.628, n=7, for ApGluR2 in L7 MN co-cultured with SN, $p<0.001$, by a two-sample t test. (D) presynaptic innervation is required for the maintenance of the clustering of glutamate receptors. ApGluR1/EGFP or ApGluR2/EGFP was expressed in L7 MN co-cultured with SN after 1 day *in vitro*. We allowed the cells to re-establish synapses for 5 days before killing SN (middle and bottom left panels). Clusters of ApGluR1 and ApGluR2 disperse over time and prominent changes in the clustering patterns could be clearly observed at 4 days after denervation (middle and bottom right panels, n=3), whereas there was very little

change in the distribution of ApGluR2 clusters in the MN innervated by intact SN at the same time point (top panels). (E) Specific interaction between pre- and postsynaptic neurons is required for the clustering of AMPA receptors. ApNR1/RFP and ApGluR1/EGFP were co-expressed in isolated L7 MN (left panels), L7 MN co-cultured with SN (middle panels) or L11 MN co-cultured with SN (right panels). ApNR1/RFP cluster in the processes of MN under all culture configurations, whereas ApGluR1/EGFP cluster only in MN that is properly innervated by presynaptic SN (middle panels). ApGLuR1/EGFP fails to cluster in either solitary L7 MN (top left panels) or mismatched L11 MN co-cultured with presynaptic SN (top right panels). The phase images of each culture condition are shown at the bottom panels. Please note that it is very common that the size of *Aplysia* neurons varies among individual cultures,. However, this does not affect the major conclusions of the experiments. For full-size images of this experiment, see Supplemental Images. (F) The enlarged images of the co-localization pattern of ApGluR1/EGFP and ApNR1/RFP receptors of Figure 1E (SN-L7 MN co-culture, middle panel). To clearly demonstrate the co-localized and non-colocalized puncta (blue and pink arrowheads), we presented the results acquired at lower laser intensity compared to that in Figure 1E. These data were quantified and presented as the percentage of AMPA receptors co-localized with NMDA receptors (74.34±2.146%, n=4).

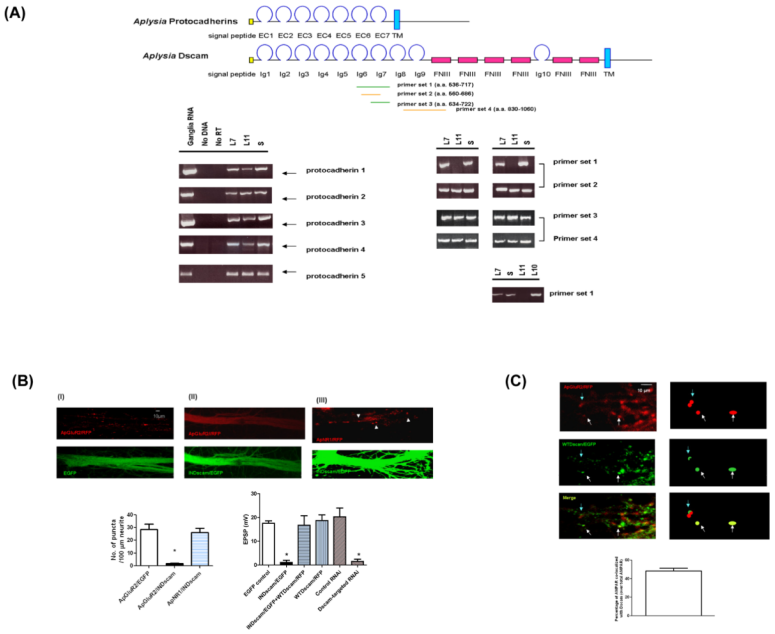

Figure 2.

ApDscam is commonly expressed in synaptically-related neurons. (A) The structural organization of *Aplysia* protocadherins and Dscam is shown in the diagram. Single cell RT/PCR showed that the pleural SN, L7 and L11 MN express comparable levels of five different protocadherins tested compared to total RNA isolated from *Aplysia* ganglia. There is no detectable signal in samples containing no cells or reverse transcriptase. The expression of ApDscam was tested using four sets of primers. The ApDscam messages in both SN and L7 MN, but not in L11 MN can be amplified by specific primer set 1 that covers Ig6 and partial Ig7 domain. However, using primer 3 that covers the entire Ig7 domain, we were able to detect comparable amounts of signal in all three cell types. Our sequencing results further suggest there is no diversity of Ig 7 domain in *Aplysia*. The difference of Dscam on L7 and L11 resides in the region before Ig7domain. This ApDscam is also expressed in L10 interneuron that makes both excitatory and inhibitory synapses with L7 MN (bottom row). In these experiments, primer set 2 and 4 were used as internal controls. (B) ApGluR2/RFP was co-expressed with EGFP or INDscam/EGFP in L7 MN on day 1 after being co-cultured with SN (panel I and II). Over-expression of INDscam/EGFP, but not EGFP abolishes clustering of ApGluR2/RFP. INDscam has no effect on the clustering of ApNR1/RFP (panel III), even when the expression level is higher than that required to abolish the clustering of ApGluR2/RFP (panel II). The quantification for these results is shown at the bottom left panel. The number of punta per 100 μm of neurites in ApGluR2/INDscam is statistically different from that in ApGluR2/EGFp and ApNR1/INDscam (1.75±0.25, 28.5±4.39 and 26.25±3.275, respectively. n=4 and $p<0.05$, by a two-sample t test). The mean EPSP in SN-MN synapses expressing EGFP alone, INDscam/EGFP alone, co-expressing INDscam/EGFP and WTDscam/RFP and expressing WTDscam/EFP alone are (mV) 17.56±0.985, 1.087±0.928, 16.73±4.018 and 18.7±2.42, respectively. The effect of INDscam/EGFP on evoked EPSP is statistically different from that in EGFP alone $p<0.002$, n=4 by a two-sample t test. These results are further supported by the RNAi approach. A mixture of 3 species of Dscam-targeted RNAi, but not the equivalent mixture of control RNAi, blocks the evoked SN-MN EPSP. The mean EPSP between SN-MN synapses in Dscam-targeted RNAi and control RNAi are 1.5±0.95 mV and 20.25±3.70 mV, respectively ($p<0.002$, n=4 by a two sample t test). (C) AMPA receptors are co-localize with WTDscam in L7 MN co-cultured with SN (arrowheads). The left panels show the confocal

images and the diagrams at the right panels illustrate several examples of superimposed puncta (arrowheads). The quantitative results are presented as the percentage of AMPA receptors which are either completely or partially co-localized with WTDscam over total AMPAR (48.25±3.11%, n=3).

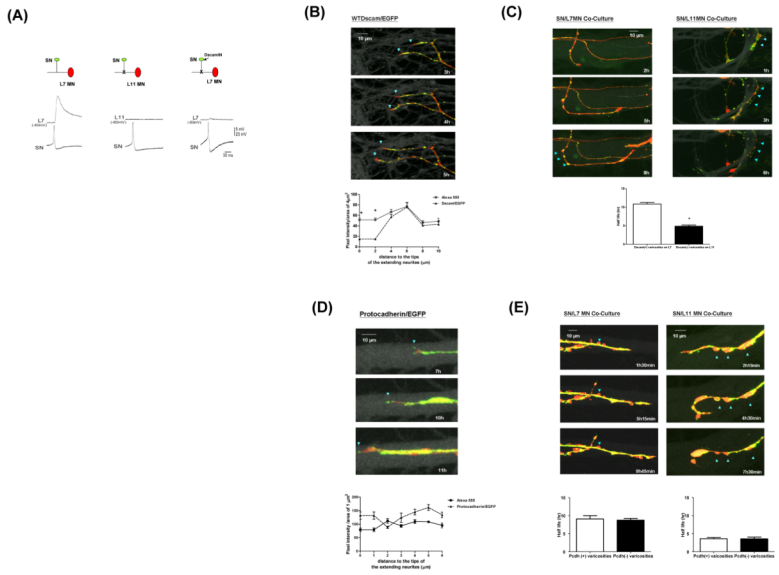

Figure 3.

Presynaptic Dscam is required for *de novo* synapse formation (A) The trace results of the EPSP recorded from MN (top row). Presynaptic overexpression of the INDscam/EGFP abolishes the evoked EPSP. (B) Dynamic changes of Dscam in the actively extending neurites. WTDscam/GFP was over-expressed in SN co-cultured with L7 or L11 MN. SN and MN were filled with the whole cell markers, dextran Alexa 555 (shown in red) and 680 (shown in gray), respectively. Data presented here are the clips of a series of time-lapse video imaging (also see Supplemental Videos 1–4). The intensity of Dscam/EGFP and Alexa 555 was quantified in a blind fashion by *Image J* and expressed as the pixel intensity of 4 μm^2. Dscam accumulates at the base, but not the leading edge of growth cones of extending neurites (left panels). The ratio of WTDscam/EGFP over Alexa 555 is 0.984, 0.882 and 0.877at 4, 6, 8 and 10 μm but decreases to 0.261 within 2 μm from the tips of growth cones, respectively ($p<0.05$, n=6 by a two-sample t test). The actual pixel intensity of each data point is in the Supplemental Figure S5. (C) SN varicosities contacting L7 MN are more stable and associated with the retention of Dscam compared to those on L11 MN (blue arrowheads, the average half life is 10.858h±0.404 and 4.857h±0.34, respectively. p, 0.001, n=7 by a two sample t test). (D) Protocadherin/EGFP (Pcdh/EGFP) was over-expressed in SN co-cultured with L7 or L11 MN (also see Supplemental Videos 5–8). In contrast to Dscam, protocadherin often accumulates at the leading edge of growing axons (The ratio of Pcdh/EGFP over Alexa 555 is 1.657±0.058 and 0.7967±0.024 at 1 and 2 μm from the tips of growing axons, $p<0.05$, n=5 by two sample t tests and the ratio at 3, 4, 5, and 6μm are 1.317±0.136, 1.32±0.085, 1.49± 0.013 and 1.412±0.044). Images shown here are enlarged for the clarity of the tips of growing axons. (E) The presence of Pcdh/EGFP is not directly associated with the stability of presynaptic varicosities. Some of the stable varicosities in SN-L7 co-culture do not contain significant levels of Pcdh/EGFP (arrowheads, left panels). Some of the unstable varicosities in SN-L11 co-culture contain significant levels of Pcdh/EGFP (arrowheads, right panels). The quantification results are shown at bottom panels. The average half life of Pcdh(+) and Pcdh(−) SN varicosities on L7 MN is 9.1 h±0.87 and 8.75 h±0.48, respectively. The average half life of SN varicosities on L11 MN is 3.575 h±0.36 and 3.525 h±0.53.

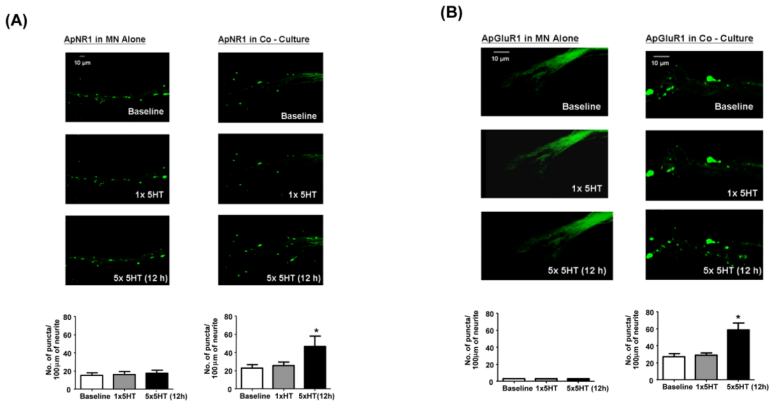

Figure 4.

LTF but not STF is associated with the remodeling of glutamate receptors. ApNR1/EGFP or ApGluR1/EGFP was expressed in L7 MN alone or co-cultured with SN after 1 day *in vitro* (4A and 4B, respectively). Cells were stimulated with 5-HT on day 5 (top panels). Induction of STF does not lead to any significant redistribution of ApNR1 and ApGluR1 in L7 MN alone (4A and 4B, middle left panels) or co-cultured with SN (4A and 4B, middle right panels). By contrast, induction of LTF is accompanied by remodeling of ApNR1 and ApGluR1 in L7 MN co-cultured with presynaptic SN (4A and 4B, bottom right panels) but not in L7 MN alone (4A and 4B, bottom left panels). ApGluR1 exhibits a diffuse but gradient distribution in L7 MN alone (4B, left panels, images were acquired using laser power of 1.5 mW). For ApNR1 in L7 MN alone, the numbers of puncta per 100 μm of neurite are 15.33±2.906 before treatment, 16.00±3.215 at 10 min after 1xHT and 17.67±3.18 at 12h after 5×5-HT, n=3. There is no statistical difference between these groups, $p>0.05$ by a one-sample t test. For ApNR1 in L7 MN co-cultured with SN, the number of puncta/100 μm are 22.80±3.839 and 25.40±4.00 before and at 10 min after 1×5-HT ($p>0.05$). However, the value at 12 h after 5×5-HT increases to 47.40±8.733, n=3 ($p<0.05$). For ApGluR1, the number of puncta/100 μm are 27.00±3.60 before treatment and remains 28.67±3.18 at 10 minutes after 1xHT ($p>0.05$, by a one-sample t test) and increases to 61.67±7.625 at 12h after 5×5-HT, n=3 ($p<0.05$).

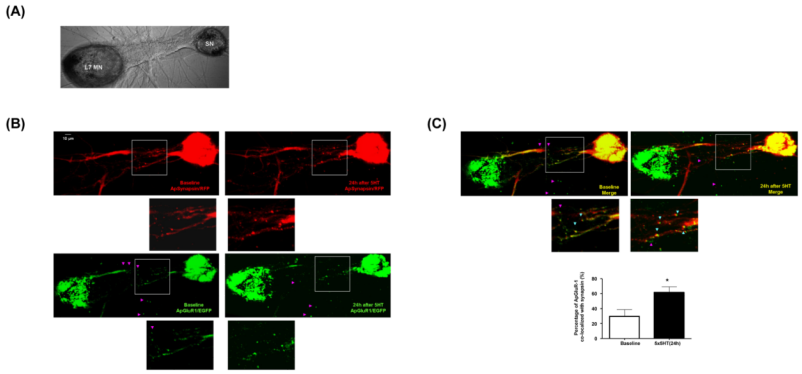

Figure 5.

LTF-associated formation of new SN to MN synapses. (A) The phase Image of SN and L7 MN co-culture. DNAs encoding ApSynapsin/RFP and ApGluR1/EGFP were injected into SN and L7 MN, respectively. (B and C) The distribution of ApSynapsin/RFP and ApGluR1/RGFP at baseline and 24h after 5-HT treatment is shown at the left and right panels, respectively. The insets in each panels are enlarged and shown right below the corresponding images. There is a high percentage of non-colocalized signals outside of the major processes of L7 MN (pink arrowheads), whereas the signals along the initial segment of L7 MN (insets) have higher percentage of co-localization (blue arrowheads).. The percentage of ApGluR-1 puncta co-localized with ApSynapsin are 29.50±8.977% before treatment and 61.67±7.265% at 24 h after 5×5-HT, n=5, $p<0.05$, by a one-sample t test). The cell bodies, but not the processes of *Aplysia* neurons are prone to emit autofluorescence. In this experiment, the autofluorescence is detectable with EGFP, but not RFP signals. For full size results, see Supplemental Images.

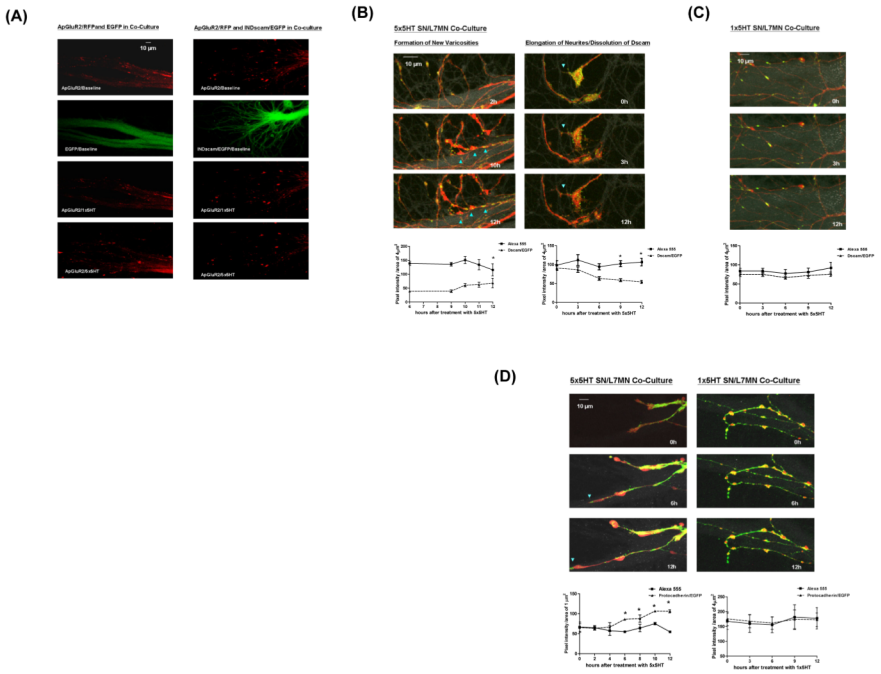

Figure 6.

Dscam is involved in LTF-associated remodeling of SN to MN synapses. (A) ApGluR2/RFP was expressed in L7 MN on day 1 after co-cultured with SN. INDscam/EGFP or EGFP was then expressed in the same L7 MN on day 4. The distribution of ApGluR2/RFP and the evoked EPSP were then monitored at 10 min or 12 h after treatment with 1 pulse or 5 pulses of 5-HT, respectively. The effects of INDscam on the expression of STF and LTF are summarized in Table 2. Overexpression of INDscam postsynaptically or INDscam presynaptically abolishes 5-HT-induced LTF compared to EGFP alone group (LTF(II)(1,3,5), $p<0.01$, $n=4$, by a two- sample t test), but has no effect on STF (STF(II) (1–3), $p>0.05$, $n=4$ by a two-sample t test). Moreover, in the absence of 5-HT, INDscam and EGFP have no significant effect on the EPSP during the same time period (LTF(I)(2,3) in Table 2). The effect of INDscam on the induction of LTF can be rescued by co-expression with WTDscam/RFP both pre- and postsynaptically (LTF(II)(4,6) in Table 2). Over-expression of WTDscam/RFP alone has no effect on the expression of LTF (LTF(II)(2) in Table 2). Moreover, knocking down the expression levels of presynaptic or postsynaptic Dscam blocks LTF but not STF (LTF(II)(7–10) and STF(II)(4–6) in Table 2). The (%) change in EPSPs for Dscam RNAi group in the induction of LTF is statistically different from control RNAi, $p<0.0001$, $n=4$ by a two sample t test. However, in the absence of 5-HT, there is no significant change in the EPSP in either groups during the same time period (LTF(I)(4,5) in Table 2). (B) Induction of LTF evokes two types of remodeling in SN. Left panels illustrate the formation of new varicosities and consequent enrichment of Dscam (the ratio of the pixel intensity of Dscam/EGFP over Alexa 555 increases from 0.312 at baseline to 0.568 at 12h after induction of LTF, $p<0.05$, $n=4$ by a one-sample t test). The actual pixel intensity of each data point is in the Supplemental Figure S5. Right panels show axonal sprouting resumes after dissolution of Dscam aggregates at the neuritic terminals (the ratio of the pixel intensity of Dscam/EGFP over Alexa 555 decreases from 0.922 at baseline to 0.50 at 12h after induction of LTF, $p<0.05$, $n=6$ by a one-sample t test.) Induction of STF does not trigger any discernible redistribution of Dscam. (D) Induction of LTF triggers re-targeting of Pcdh/EGFP to the tips of the growing axons (the ratio of the pixel intensity of Protocadherin/EGFP over Alexa 555 at 1μm from the tips of the growing axons is 1.022±0.07 (0h), 0.987±0.09 (2h), 1.192±0.143 (4h), 1.57±0.0 (6h), 1.393±0.052 (8h),

1.428±0.06 (10h) and 1.94±0.13 (12h)). The results from 6 to 12 h after stimulation is significantly different from baseline, $p<0.05$, $n=4$ by a one-sample t test. However, induction of STF does not evoke any discernible changes in the distribution of Pcdh/EGFP (right panel). The ratio of the pixel intensity of Pcdh/EGFP over Alexa 555 is 1.239±0.18 (0h), 1.268±0.172 (3h), 1.141±0.137 (6h), 1.155±0.19 (9h) and 1.19±0.24 (12h).

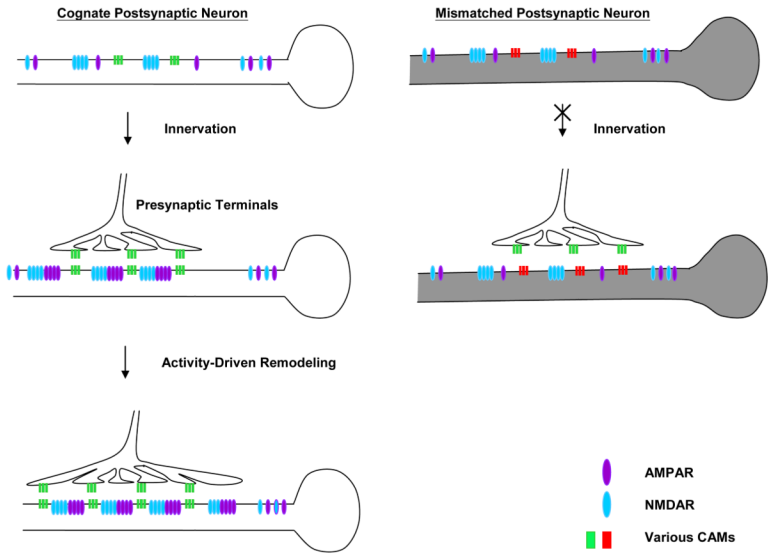

Figure 7.

Possible mechanisms of Dscam-mediated synapse formation. Prior to presynaptic innervation, NMDA receptors cluster randomly along the postsynaptic surface. Upon presynaptic innveration, the trans-synaptic signaling mediated by various cell adhesion molecules (e.g. Dscam) promotes the subsequent organization of postsynaptic AMPA receptors and the stabilization of presynaptic varicosities. The induction of LTF can reutilize aspects of the developmental program. In response to the induction of LTF, postsynaptic Dscam regulates the remodeling of AMPA receptors whereas an enrichment of presynaptic Dscam stabilizes newly formed varicosities to promote the formation of new functional synaptic connections.

Table 1

	WTDscam/EGFP	**Protocadherin/EGFP**
***De Novo* Synapse Formation**		
Morphology	Punctate	Punctate and tubular structures
Growth Cones	Concentrated at the base of growth cones	Often targeted to the tips of growth cones
Association with Stable Varicosities	Yes	No
Accumulation at terminal varicosities	Yes	No. The signals of protocadherin/EGFP can be found along the entire neurites
Learning-Related Synapse Formation		
Terminal Varicosities	Dissolution of WT Dscam/EGFP aggregates	Re-targeted to the tips of growth cones
New Varicosities	Accumulation of WT Dscam/EGFP	N/A

Table 2

	(%) changes of EPSP
Short-Term Facilitation (STF):	
I. mock-treated	−21±3.342
II. 1×5-HT treated	
(1) EGFP (post)	52.5± 3.23
(2) INDscam/EGFP (post)	68.5 ± 11
(3) INDscam/EGFP (pre)	66.4±2.03
(4) Control RNAi (post)	57.0±3.94
(5) Dscam-targeted RNAi (post)	55.75±2.56
(6) Dscam-targeted RNAi (pre)	53.75±2.92
Long-Term Facilitation (LTF):	
I. mock-treated	
(1) no transgene	26.75±2.69
(2) EGFP (post)	25.75±1.93
(3) INDscam/EGFP (post)	26.00±2.49
(4) Control RNAi (post)	30.5±3.57
(5) Dscam-targeted RNAi (post)	29.25±2.4
II. 5×5HT treated	
(1) EGFP (post)	140.3±4.479
(2) WTDscam/RFP (post)	138.5±4.875
(3) INDscam/EGFP (post)	44.75±4.768 (*)
(4) INDscam/EGFP+WTDscam/RFP (post)	131.3±6.575
(5) INDscam/EGFP (pre)	40.25±2.496 (*)
(6) INDscam/EGFP+WTDscam/RFP (pre)	133±6.442
(7) Control RNAi (post)	134.0±4.183
(8) Dscam-targeted RNAi (post)	41.25±4.27(*)
(9) Control RNAi (pre)	121.3±4.535
(10) Dscam-targeted RNAi (pre)	33.5±5.236 (*)

Table 3

Nomenclature of *Aplysia* glutamate receptors, protocadherins and Dscam

This Study (Gene Bank Accession No.)	Others (Gene Bank Accession No.)	Database of *Aplysia* Transcriptome (Clones)
ApGluR1 (DQ222204)	Aplysia GluR4 (AY 289942)	
ApGluR2 (DQ222205)	Aplysia GluR3 (AY 289941)	
NMDA-like receptor	NMDA-like receptor (AY 315153,AY 163562)	
Protocadherin 1	Cadherin-like 1 (AF 364180)	CNSN01-F-137737-501 APL_all_052305.15407.c1
Protocadherin 2	Cadherin-like 2 (AF 527992)	CNSN01-F-143518-501 APL_all_052305.11406.c2
Protocadherin 3	Cahderin-like 3 (AF 527993)	APL_all_052305.122.c3
Protocadherin 4	N/A	CNSN01-F-047631-501 APL_all_052305.5701.c1
Protocadherin 5	N/A	APL_all_052305.12851.c1
Dscam (EF523610)	N/A	

Note: The database of *Aplysia* transcriptome is presented at the following websites: http://aplysia.uf-genome.org and http://aplysia.cu-genome.org

Table 4

Summary of the cloning strategy of the DNA constructs used in this study

Constructs	Cloning Strategy
1. ApGluR1/EGFP	EGFP is inserted into an artificial EcoRV site which is created after the 3rd amino acid down the putative signal peptide.
2. ApGluR2/EGFP	Same strategy as ApGluR1/EGFP
3. ApNR1/EGFP	EGFP is inserted into the Stu I site which is located at the 4th amino acid down the putative signal peptide.
4. ApNR1/RFP	Same strategy as above except that EGFP is replaced by RFP
5. ApDscam/EGFP	ApDscam is cloned into N1-EGFP vector [1]
6. ApDscam/RFP	ApDscam is cloned into N1-RFP vector[1]
7. INDscam/EGFP	The intracellular domain of Dscam (a.a. 1670 to 1963) is cloned into the C1-EGFP vector[1]
8. ECDscam/EGFP	DNA encoding the extracellular and transmembrane domains of Dscam (a.a. 1-1673) is cloned into the N1-EGFP vector[1]
9. ApProtocadherin/EGFP	ApProtocadherin is fused with EGFP by PCR
10. ApSynapsin/RFP	ApSynapsin is inserted between HindIII and SacI sites of DsRed C1 vector[1]

Note: The fluorescent protein vectors were acquired from Clontech, CA. These fusion constructs were subcloned into pNex-3 vector for the expression in *Aplysia* neurons.

Table 5

List of Stealth® RNAi sequences

Stealth RNAi (sense strand)	Control RNAi (sense strand)
1. 994 (start site of the RNAi) GAC UAC AUC UGU ACU GGC GUC AAU A	1. Control 994 GAC CUA CAU GUG GUC CUG CAA UAU A
2. 2737 (start site of this RNAi) GGU AAC GGA GUA CUG GUC AAC UAC U	2. Control 2737 GGU AGG CCA UGU GGU CAA CUA AAC U
3. 5072 (start site of this RNAi) CGU CCU UGA UGA ACG ACC UUG ACA A	3. Control 5072 CGU AGU UAA GUC AGC GUU CAC CCA A

Note: Stealth RNAi sequences were designed based on the algorithm provided by Invitrogen, CA. This table shows only the sense strand of the RNAi duplex. To determine the effects of these RNAi during *de novo* formation of SN-MN synapses, a mixture of these RNAi (6.7 μM) was microinjected into *Aplysia* neurons at 6 h after plating the cells *in vitro* and thereafter every 48 h. To determine the effect of these RNAi on the expression of LTF, a mixture of these RNAi was microinjected into mature *Aplysia* neuronal culture on day 4. Cells were then stimulated with 5-HT to induce facilitation.

Table 6

Primers for single cell RT/PCR

Genes	Primers (5′-3′) for PCR	
ApGluR1	F:AACTATTCTAAACATTTT	R:GCTAGACGTGACATATCT
ApGluR2	F:GTGTACAAGTCCAAGATC	R:CGAGTCGACTCCAGCGGT
	Nested primer pair	
	F1:CTTCATGAGTCTTGGGAT	R1: TCCCGGAGATGATGGTGC
	F2: CTCCATCATGATCAAGCG	F2: CATATTGGATGTCGGTCT
ApNR1	F:TGGCGCTAGTGCTCTATC	R:TTTGCTCTTCTCGTTGCT
ApSynapsin	F1: CTGTGGTCAAATCCAGAA	R1; AGTAGGGTCATGGACGAA
	F2: GTTCAAGCCAGACTTTGT	R2; GGAAGTCGTAGTGGTTGT
Protocadherin 1	F1: GTGAGAGATGAGAACGAC	R1:TGCTACAACAGTGAGGTT
	F2: ATGCGACGTCTTGACTGG	R2:ACAGCTCTCCTGTACTGT
Protocadherin 2	F1: GTGGAGAAGAAGATGGGT	R1:CGATATGATGGAGTCGTT
	F2: TCGGAGATCACGTTGGAT	R2:GGAGATTCGAACCGTGTT
Protocadherin 3	F1: AAGGAAGAACACGGGCAT	R1:TGTTTTAGGTGGGCTTCC
	F2: AGATAATCCTGTTGGTGG	R2:CATCACATATGCCTTGTG
Protocadherin 4	F1: AGTCACAGTCCTGGACGT	R1:CACGTCCAGTCGAAGTT
	F2: ACCACACGCCGACATTTG	R2:AGTTCCTGTGACGATGA
Protocadherin 5	F1: CGGAACTAGCAACCTATT	R1:ATTTTCGCGATCGAGCCT
	F2: CATCTAATGAACCTCCGG	R2:CCGCTGGTTCATGTGAAA
	PCR program for ApGluR1, ApGluR2, ApNR1 and protocadherins: 94°C for 1min, 55°C for 1min and 72°Cfor 1 min for 35 cycles	
ApDscam	Reverse transcription using primer R1:GTGTAGTGACAGAAGCAG Nested primer set 1	
	F1: GGGAGTACACGTGCTACG	R1:GTGTAGTGACAGAAGCAG
	F2: GAGCCTCAACAAGGTCAA	R2:GCGTTGGCTTACGTAACA
	Nested primer set 2	
	F2: GAGCCTCAACAAGGTCAA	R2:GCGTTGCCTTACGTAACA
	F3: CAAACCGTTCATCAAGCC	R3:GAATGGAGTAGTCTCCAA
	PCR program for this primer set of Dscam: 94°C for 1min, 45°C for 1min and 72°C for 1 min for 35 cycles	
	Nested primer set 3	
	F1890: GTTGTGGAACCCCCAGTTATC	
	R2195: TCCACCACCCATCTCGGGGGA	
	F1902: CCCCCAGTTATCGACCCTTTCCACTTCCGT	
	R2185: CTCGGGGGAACATCAATGTGT	
	Nested primer set 4	

Genes	Primers (5′-3′) for PCR
	F2495: CCTCGACGTAACTACACCGTG
	R3218: GCCGGGCTCTGCGTCTCC
	F2592: GGCTCTGCCATCAGCGCTCACAAC
	R3130: TGAGCGCCTGCGACCCGA
	PCR program for this primer set of Dscam: 94°C for 1min, 70°C for 1min and 72°C for 1 min for 35 cycles